Commun. Comput. Phys.
doi: 10.4208/cicp.OA-2017-0090

Vol. **23**, No. 3, pp. 640-664
March 2018

An Immersed Boundary Method for Simulating Interfacial Flows with Insoluble Surfactant in Three Dimensions

Yunchang Seol[1,*], Shih-Hsuan Hsu[2] and Ming-Chih Lai[2]

[1] *National Center for Theoretical Sciences, No. 1, Sec. 4, Road. Roosevelt, National Taiwan University, Taipei 10617, Taiwan.*
[2] *Department of Applied Mathematics, National Chiao Tung University, 1001 Ta Hsueh Road, Hsinchu 300, Taiwan.*

Received 12 April 2017; Accepted (in revised version) 29 June 2017

Abstract. In this paper, an immersed boundary (IB) method for simulating the interfacial flows with insoluble surfactant in three dimensions is developed. We consider a doubly periodic interface separating two fluids where the surfactant exists only along the evolving interface. An equi-arclength parametrization is introduced in order to track the moving interface and maintain good Lagrangian meshes, so stable computations can be performed without remeshing. This surface mesh-control technique is done by adding two artificial tangential velocity components into the Lagrangian marker velocity so that the Lagrangian markers can be equi-arclength distributed during the time evolution. As a result, the surfactant equation on the interface must be modified based on the new parametrization. A conservative scheme for solving the modified surfactant equation has been developed and proved to satisfy the total surfactant mass exactly in discrete level. A series of numerical experiments consisting of the validation of Lagrangian mesh control technique, the convergence study, the study of self-healing dynamics, and the simulations of two-layer fluids under Couette flow have been conducted to test our present numerical scheme.

AMS subject classifications: 35Q35, 65M06, 76D45
Key words: Insoluble surfactant, a conservative scheme, mesh control, interfacial flow, Navier-Stokes flow, immersed boundary method.

1 Introduction

Surfactant is a typical compound of amphiphilic molecules with hydrophilic heads and hydrophobic tails. It adheres to the fluid interface and changes the surface tension accordingly. So, in the presence of surfactant, the dynamics of interfacial flows can be

*Corresponding author. *Email addresses:* ycseol@ntu.edu.tw (Y. Seol), narisawa.am02g@g2.nctu.edu.tw (S.-H. Hsu), mclai@math.nctu.edu.tw (M.-C. Lai)

 ©2018 Global-Science Press

dramatically altered in complex ways due to the variable surface tension. For instance, a recent work of Pan et al. [37] demonstrates that by simply adding a small amount of surfactant, one can manipulate the impact outcome of droplet collision from coalescence to bouncing. Surfactant also plays a crucial role in numerous industrial applications including oil recovery, ore extraction, emulsification, pharmaceutical, and food industry [24], etc. Nowadays, we are benefited from scientific success with applications to its practical use; however, the understanding of surfactant effects is far from being complete.

For the past two decades, the interfacial flows with insoluble and soluble surfactant have been extensively studied by numerical computations. Those numerical methods are strongly relevant to how the interface is represented and how the surfactant convection-diffusion equation is solved along the evolving interface. For the soluble surfactant case, another coupling bulk convection-diffusion equation needs to be solved in one of bulk regions. In early computational models of surfactant problems, the boundary integral formulations in Stokes flow were extensively employed [12,28,30,31,40,46], refer to [35] for a review. In order to take the inertia effect into account, various numerical methods were proposed to incorporate with Navier-Stokes equations. These methods are based upon volume-of-fluid (VOF) [4, 11, 21], front-tracking method [9, 32, 33], immersed boundary method [7, 25–27], level-set [47, 48], and arbitrary Lagrangian-Eulerian (ALE) finite element method [3, 15–17, 19, 36]. Apart from the methods listed above, other numerical studies include diffuse-interface method [43], segmented projection method [22, 23], lattice Boltzmann method [13], moving particle semi-implicit method [14], and smoothed particle hydrodynamics (SPH) method [1] etc. Some hybrid approaches combining two different methods were proposed as well [6, 29, 49, 51]. In this paper, we extend the third author's previous 2D [25, 26] and axisymmetric [27] works and propose a three-dimensional immersed boundary (IB) method for simulating the evolution of a deforming interface with insoluble surfactant.

As known, solving the surfactant convection-diffusion equation on an evolving interface has already been a numerical challenge, especially in three-dimensional space. From the authors point of view, there are two major numerical issues to be considered carefully. (1) How to maintain the interfacial mesh quality to avoid Lagrangian markers clustering and surface mesh distortion without re-meshing? (2) How to guarantee that the total surfactant mass is conserved along the evolving interface without re-scaling? In this paper, we aim to propose a numerical scheme that can handle both issues systematically for an evolving free interface. Our numerical approach is outlined as follows. We first assume a doubly periodic interface separating two fluids where the surfactant exists only along the evolving interface. An equi-arclength parametrization is introduced in order to track the moving interface and maintain good Lagrangian meshes, so stable computations can be performed without re-meshing. This surface mesh-control technique is done by adding two artificial tangential velocity components into the Lagrangian marker velocity so that the Lagrangian markers can be equi-arclength distributed during the time evolution. As a result, the surfactant equation on the interface must be modified based on the new parametrization. A conservative scheme for solving the modified surfactant equation

has been developed and proved to satisfy the total surfactant mass exactly in discrete level. We then apply the developed scheme to simulate the problems of interfacial flows with insoluble surfactant.

The rest of this paper is organized as follows. In the next section, we present the equations of motion under the immersed boundary framework. We also describe the related contents of surface differential geometry needed in our mathematical formulation. In Section 3, an equi-arclength parametrization for a deforming interface is introduced and the modified surfactant concentration equation is derived accordingly. In Section 4, we first develop a conservative scheme for solving the modified surfactant equation and then outline the time-stepping scheme for solving the whole fluid equations with insoluble surfactant. A series of numerical tests to validate our present scheme is given in Section 5 which is followed by some conclusions and future work in Section 6.

2 Equations of motion

In this section, we consider the flow of two immiscible viscous incompressible Navier-Stokes fluids in a three-dimensional domain Ω. The sharp interface Σ separating those two fluids is assumed to be doubly periodic in the horizontal x and y directions while it is free in the z direction. Besides the external applying flow, the motion of the interface and fluids is mainly driven by the surface tension along the free interface where an insoluble surfactant is distributed and varied on the interface that changes the surface tension in a timely fashion. Using the immersed boundary (or front-tracking) formulation, the fluid variables are represented in Eulerian manner while the interface quantities are represented in Lagrangian manner so the dimensionless governing equations for the above two-phase flow with insoluble surfactant can be written as one whole fluid system as follows [9,25].

$$\frac{\partial \mathbf{u}}{\partial t}+(\mathbf{u}\cdot\nabla)\mathbf{u}=-\nabla p+\frac{1}{Re}\nabla\cdot\Big(\mu\Big(\nabla\mathbf{u}+(\nabla\mathbf{u})^T\Big)\Big)+\frac{\mathbf{f}}{ReCa}\ \text{ in }\Omega, \tag{2.1}$$

$$\nabla\cdot\mathbf{u}=0\ \text{ in }\Omega, \tag{2.2}$$

$$\mathbf{f}(\mathbf{x},t)=\int_\Sigma \mathbf{F}(\alpha,\beta,t)\delta(\mathbf{x}-\mathbf{X}(\alpha,\beta,t))\,\mathrm{d}A\ \text{ in }\Omega, \tag{2.3}$$

$$\frac{\partial \mathbf{X}}{\partial t}(\alpha,\beta,t)=\mathbf{U}(\alpha,\beta,t)=\int_\Omega \mathbf{u}(\mathbf{x},t)\delta(\mathbf{x}-\mathbf{X}(\alpha,\beta,t))\,\mathrm{d}\mathbf{x}\ \text{ on }\Sigma, \tag{2.4}$$

$$\mathbf{F}(\alpha,\beta,t)=\nabla_s\sigma-2\sigma H\mathbf{n},\qquad \sigma(\alpha,\beta,t)=\sigma_0(1-\eta\Gamma(\alpha,\beta,t))\ \text{ on }\Sigma, \tag{2.5}$$

$$\frac{\partial \Gamma}{\partial t}(\alpha,\beta,t)+(\nabla_s\cdot\mathbf{U})\Gamma(\alpha,\beta,t)=\frac{1}{Pe_s}\Delta_s\Gamma(\alpha,\beta,t)\ \text{ on }\Sigma, \tag{2.6}$$

Eqs. (2.1) and (2.2) are the Navier-Stokes equations in which $\mathbf{u}$ is the velocity and p is the pressure. Here we assume both fluids have equal density but different viscosity denoting the upper fluid viscosity by μ^+ and the lower by μ^-. So the Reynolds number is defined by $Re=\rho VL/\mu^+$ where ρ,V and L are the corresponding scales for the density,

velocity and length. We assume $\mu^- \geq \mu^+$ throughout this paper although this is not a restriction to our present method. Another dimensionless number in fluid equations is the capillary number $Ca = \mu^+ V/\sigma_0$ where σ_0 represents the constant surface tension without surfactant. The interface $\Sigma(t)$ between two fluid layers is a two-dimensional surface in Ω, represented by $\Sigma(t) = \{\mathbf{X}(\alpha,\beta,t) | 0 \leq \alpha \leq 2\pi, 0 \leq \beta \leq 2\pi\}$, where (α,β) are the Lagrangian coordinates. Throughout the paper, the effect of gravity is neglected so the only force in Eulerian fluid domain arises from the spreading of interfacial force $\mathbf{F}$ via the Dirac delta function $\delta(\mathbf{x}) = \delta(x)\delta(y)\delta(z)$ as shown in Eq. (2.3). Similarly, the interfacial velocity $\mathbf{U}$ is also interpolated from the local Eulerian fluid velocity via the delta function in Eq. (2.4). The interfacial force $\mathbf{F}$ in Eq. (2.5) consists of tangential and normal components; namely, the surface gradient of tension $\nabla_s \sigma$ (Marangoni force) and the mean curvature force $2\sigma H\mathbf{n}$ (capillary force). Here, H is the mean curvature of the free interface and the normal vector $\mathbf{n}$ is chosen pointing into the upper fluid direction. The surface tension related to the surfactant concentration is determined by the Langmuir equation of state in Eq. (2.5) where η $(0 \leq \eta < 1)$ is the dimensionless elasticity number that quantifies the sensitivity of interfacial tension to the changes of surfactant concentration as in [34]. The surfactant is insoluble and its concentration Γ satisfies the convection-diffusion equation [41] as in (2.6), where Pe_s is the surface Peclet number. Here $\Gamma(\alpha,\beta,t)$ is defined in Lagrangian coordinates, so $\frac{\partial \Gamma}{\partial t}$ is the material derivative. To be complete, the above governing equations (2.1)-(2.6) must be accompanied with suitable initial and boundary conditions.

In the following, we shall introduce some preliminary surface differential geometry [10] to express the mathematical forms for the surface gradient ∇_s, surface divergence $\nabla_s \cdot$, and surface Laplace Δ_s operators used in above formulation. For a surface patch $\mathbf{X}(\alpha,\beta)$ at some fixed time, the coefficients of the first fundamental form are defined by

$$E = \mathbf{X}_\alpha \cdot \mathbf{X}_\alpha, \quad F = \mathbf{X}_\alpha \cdot \mathbf{X}_\beta, \quad G = \mathbf{X}_\beta \cdot \mathbf{X}_\beta,$$

where the subscripts α and β of a function denote its partial derivatives of the function with respect to α and β, respectively. So the local area stretching factor can be written as $|\mathbf{X}_\alpha \times \mathbf{X}_\beta| = \sqrt{EG - F^2}$. We define the unit normal vector as $\mathbf{n} = \mathbf{X}_\alpha \times \mathbf{X}_\beta / |\mathbf{X}_\alpha \times \mathbf{X}_\beta|$, where $|\cdot|$ stands for the usual Euclidean norm. The coefficients of the second fundamental form are defined by

$$L = \mathbf{X}_{\alpha\alpha} \cdot \mathbf{n} = -\mathbf{X}_\alpha \cdot \mathbf{n}_\alpha, \quad M = \mathbf{X}_{\alpha\beta} \cdot \mathbf{n} = -\mathbf{X}_\alpha \cdot \mathbf{n}_\beta = -\mathbf{X}_\beta \cdot \mathbf{n}_\alpha, \quad N = \mathbf{X}_{\beta\beta} \cdot \mathbf{n} = -\mathbf{X}_\beta \cdot \mathbf{n}_\beta.$$

So the mean curvature of the surface can be written as $H = \frac{-GL - EN + 2FM}{2(EG - F^2)}$.

Using those fundamental forms, the surface gradient $\nabla_s \sigma$ of a scalar function σ can be represented by

$$\nabla_s \sigma = \frac{G\sigma_\alpha - F\sigma_\beta}{EG - F^2}\mathbf{X}_\alpha + \frac{E\sigma_\beta - F\sigma_\alpha}{EG - F^2}\mathbf{X}_\beta, \tag{2.7}$$

while the surface divergence $\nabla_s \cdot \mathbf{U}$ of a vector field $\mathbf{U}$ can be represented by

$$\nabla_s \cdot \mathbf{U} = \frac{G\mathbf{U}_\alpha - F\mathbf{U}_\beta}{EG - F^2} \cdot \mathbf{X}_\alpha + \frac{E\mathbf{U}_\beta - F\mathbf{U}_\alpha}{EG - F^2} \cdot \mathbf{X}_\beta. \tag{2.8}$$

For a surface vector field $\mathbf{U}^s = P\mathbf{X}_\alpha + Q\mathbf{X}_\beta$, its surface divergence can also be alternatively written as

$$\nabla_s \cdot \mathbf{U}^s = \frac{1}{|\mathbf{X}_\alpha \times \mathbf{X}_\beta|}\left[\frac{\partial}{\partial\alpha}\left(|\mathbf{X}_\alpha \times \mathbf{X}_\beta| P\right) + \frac{\partial}{\partial\beta}\left(|\mathbf{X}_\alpha \times \mathbf{X}_\beta| Q\right)\right]. \tag{2.9}$$

This formula can be derived by using direct substitution of $\mathbf{U}^s$ into Eq. (2.8). After combining two operators in Eqs. (2.7) and (2.9), the surface Laplacian (or Laplace-Beltrami operator) of Γ has the form

$$\Delta_s \Gamma = \nabla_s \cdot \nabla_s \Gamma = \frac{1}{|\mathbf{X}_\alpha \times \mathbf{X}_\beta|}\left[\left(\frac{G\Gamma_\alpha - F\Gamma_\beta}{|\mathbf{X}_\alpha \times \mathbf{X}_\beta|}\right)_\alpha + \left(\frac{E\Gamma_\beta - F\Gamma_\alpha}{|\mathbf{X}_\alpha \times \mathbf{X}_\beta|}\right)_\beta\right]. \tag{2.10}$$

3 An equi-arclength parametrization for a deforming free surface and the modified surfactant equation

As mentioned in the Introduction, three-dimensional interfacial flow simulations pose numerical challenges to track the free surface using the underlying surface meshes. More precisely speaking, it is difficult to maintain a surface parametrization using global coordinates that keeps the underlying mesh in good quality (without too much mesh distortion) during the time evolution. In this paper, we propose an approach to maintain such global parametrization by first choosing an equi-arclength parametrization along two principal tangential directions and then try to maintain the property by adding appropriate artificial tangential velocities. The validity of such mechanism is theoretically ensured because the interfacial shape remains unchanged by adding any tangential velocity, while artificial normal velocity will change the shape accordingly which results in undesired dynamics. This is an extension to the earlier work [26] on a curve interface in two-dimensional interfacial flow by the third author and his coworkers. By exploiting this equi-arclength technique, one can see the Lagrangian markers to track the interface is indeed uniformly distributed [26]. One should notice that, the idea of adding two tangential velocities to the surface velocity to preserve some parametrization properties is not new; for instance, a generalized isothermal parametrization was introduced in 3D boundary integral computations for incompressible Darcy's flow with surface tension in [2]. More relevant works to study different flows using the same idea can be found in the references therein.

To proceed, we modify the surface evolutional equation (2.4) by adding two tangential velocities as

$$\frac{\partial \mathbf{X}}{\partial t}(\alpha,\beta,t) = \mathbf{U}(\alpha,\beta,t) + V_1(\alpha,\beta,t)\boldsymbol{\tau}^1 + V_2(\alpha,\beta,t)\boldsymbol{\tau}^2, \tag{3.1}$$

where $\boldsymbol{\tau}^1 = \mathbf{X}_\alpha/|\mathbf{X}_\alpha|$ and $\boldsymbol{\tau}^2 = \mathbf{X}_\beta/|\mathbf{X}_\beta|$ are the unit tangent vectors satisfying $\boldsymbol{\tau}^1 \times \boldsymbol{\tau}^2 \neq 0$. The goal is to derive the two evolutional equations for V_1 and V_2 so that the equi-arclength

parametrization for the surface can be always preserved if the initial surface is chosen to have such property. Like the free interface $\mathbf{X}$, here, we assume that the velocities $\mathbf{U}, V_1, V_2$ are all 2π doubly periodic. For a surface $\mathbf{X}(\alpha,\beta,t)$, an equi-arclength parametrization in both principal tangential directions satisfies

$$\frac{\partial}{\partial\alpha}|\mathbf{X}_\alpha| = 0 \quad \text{and} \quad \frac{\partial}{\partial\beta}|\mathbf{X}_\beta| = 0,$$

for all $(\alpha,\beta)\in[0,2\pi]\times[0,2\pi]$. Thus, we have

$$|\mathbf{X}_\alpha| = \frac{1}{2\pi}\int_0^{2\pi}|\mathbf{X}_{\alpha'}|\,\mathrm{d}\alpha' \quad \text{and} \quad |\mathbf{X}_\beta| = \frac{1}{2\pi}\int_0^{2\pi}|\mathbf{X}_{\beta'}|\,\mathrm{d}\beta'. \tag{3.2}$$

Taking the time derivative in Eq. (3.2), it yields

$$|\mathbf{X}_\alpha|_t = \frac{1}{2\pi}\int_0^{2\pi}|\mathbf{X}_{\alpha'}|_t\,\mathrm{d}\alpha' \quad \text{and} \quad |\mathbf{X}_\beta|_t = \frac{1}{2\pi}\int_0^{2\pi}|\mathbf{X}_{\beta'}|_t\,\mathrm{d}\beta', \tag{3.3}$$

where $|\mathbf{X}_\alpha|_t$ can be expressed by

$$\begin{aligned}|\mathbf{X}_\alpha|_t &= \frac{\mathbf{X}_{\alpha t}\cdot\mathbf{X}_\alpha}{|\mathbf{X}_\alpha|} = \mathbf{X}_{\alpha t}\cdot\boldsymbol{\tau}^1 = (\mathbf{X}_t)_\alpha\cdot\boldsymbol{\tau}^1\\ &= \frac{\partial\mathbf{U}}{\partial\alpha}\cdot\boldsymbol{\tau}^1 + \frac{\partial V_1}{\partial\alpha} + \frac{\partial V_2}{\partial\alpha}\left(\boldsymbol{\tau}^2\cdot\boldsymbol{\tau}^1\right) + V_2\frac{\partial\boldsymbol{\tau}^2}{\partial\alpha}\cdot\boldsymbol{\tau}^1.\end{aligned}$$

Substituting the above equation into Eq. (3.3) and integrating with respect to α, we obtain

$$V_1(\alpha,\beta,t) = \frac{\alpha}{2\pi}\int_0^{2\pi}Q(\alpha',\beta,t)\,\mathrm{d}\alpha' - \int_0^{\alpha}Q(\alpha',\beta,t)\,\mathrm{d}\alpha', \tag{3.4}$$

where

$$Q(\alpha,\beta,t) = \frac{\partial\mathbf{U}}{\partial\alpha}\cdot\boldsymbol{\tau}^1 + \frac{\partial V_2}{\partial\alpha}\left(\boldsymbol{\tau}^2\cdot\boldsymbol{\tau}^1\right) + V_2\frac{\partial\boldsymbol{\tau}^2}{\partial\alpha}\cdot\boldsymbol{\tau}^1.$$

Similarly, one can derive

$$V_2(\alpha,\beta,t) = \frac{\beta}{2\pi}\int_0^{2\pi}R(\alpha,\beta',t)\,\mathrm{d}\beta' - \int_0^{\beta}R(\alpha,\beta',t)\,\mathrm{d}\beta', \tag{3.5}$$

where

$$R(\alpha,\beta,t) = \frac{\partial\mathbf{U}}{\partial\beta}\cdot\boldsymbol{\tau}^2 + \frac{\partial V_1}{\partial\beta}\left(\boldsymbol{\tau}^1\cdot\boldsymbol{\tau}^2\right) + V_1\left(\frac{\partial\boldsymbol{\tau}^1}{\partial\beta}\cdot\boldsymbol{\tau}^2\right).$$

In the above derivations, we impose the boundary conditions for $V_1(0,\beta,t) = V_2(\alpha,0,t) = 0$, implying that at these boundary points, no additional tangential velocities are needed in their corresponding directions.

Since the surfactant transports and diffuses along the interface, by taking the new surface parametrization Eq. (3.1) into account, the original surfactant equation (2.6) must be modified to

$$\frac{\partial \Gamma}{\partial t} - (V_1\boldsymbol{\tau}^1 + V_2\boldsymbol{\tau}^2)\cdot\nabla_s\Gamma + (\nabla_s\cdot\mathbf{U})\Gamma = \frac{1}{Pe_s}\Delta_s\Gamma.$$

Multiplying the surface stretching factor $|\mathbf{X}_\alpha\times\mathbf{X}_\beta|$ on both sides of the above equation and using the following identity derived in [38],

$$\frac{\partial|\mathbf{X}_\alpha\times\mathbf{X}_\beta|}{\partial t} = |\mathbf{X}_\alpha\times\mathbf{X}_\beta|\nabla_s\cdot\frac{\partial\mathbf{X}}{\partial t} = |\mathbf{X}_\alpha\times\mathbf{X}_\beta|\nabla_s\cdot\left(\mathbf{U}+V_1\boldsymbol{\tau}^1+V_2\boldsymbol{\tau}^2\right),$$

we obtain

$$\begin{aligned}&\frac{\partial\Gamma}{\partial t}|\mathbf{X}_\alpha\times\mathbf{X}_\beta| - |\mathbf{X}_\alpha\times\mathbf{X}_\beta|(V_1\boldsymbol{\tau}^1+V_2\boldsymbol{\tau}^2)\cdot\nabla_s\Gamma\\ &\quad+\frac{\partial|\mathbf{X}_\alpha\times\mathbf{X}_\beta|}{\partial t}\Gamma - |\mathbf{X}_\alpha\times\mathbf{X}_\beta|\left[\nabla_s\cdot\left(V_1\boldsymbol{\tau}^1+V_2\boldsymbol{\tau}^2\right)\right]\Gamma = \frac{|\mathbf{X}_\alpha\times\mathbf{X}_\beta|}{Pe_s}\Delta_s\Gamma.\end{aligned}$$

By putting the terms together, one can simplify the above equation as

$$\frac{\partial\left(\Gamma|\mathbf{X}_\alpha\times\mathbf{X}_\beta|\right)}{\partial t} - |\mathbf{X}_\alpha\times\mathbf{X}_\beta|\nabla_s\cdot\left[\left(V_1\frac{\mathbf{X}_\alpha}{|\mathbf{X}_\alpha|}+V_2\frac{\mathbf{X}_\beta}{|\mathbf{X}_\beta|}\right)\Gamma\right] = \frac{|\mathbf{X}_\alpha\times\mathbf{X}_\beta|}{Pe_s}\Delta_s\Gamma.$$

Using the formulas for the surface divergence in Eq. (2.9) and the surface Laplacian in Eq. (2.10), we have

$$\begin{aligned}&\frac{\partial\left(\Gamma|\mathbf{X}_\alpha\times\mathbf{X}_\beta|\right)}{\partial t} - \left[\left(\frac{|\mathbf{X}_\alpha\times\mathbf{X}_\beta|V_1\Gamma}{\sqrt{E}}\right)_\alpha + \left(\frac{|\mathbf{X}_\alpha\times\mathbf{X}_\beta|V_2\Gamma}{\sqrt{G}}\right)_\beta\right]\\ &=\frac{1}{Pe_s}\left[\left(\frac{G\Gamma_\alpha - F\Gamma_\beta}{|\mathbf{X}_\alpha\times\mathbf{X}_\beta|}\right)_\alpha + \left(\frac{E\Gamma_\beta - F\Gamma_\alpha}{|\mathbf{X}_\alpha\times\mathbf{X}_\beta|}\right)_\beta\right].\end{aligned} \tag{3.6}$$

One can immediately see that the above modified surfactant equation is written in a form of conservation law which has the advantage of designing a conservative scheme. Indeed, in next section, Eq. (3.6) will be discretized by a conservative finite difference scheme and numerical evidences in Section 5 demonstrate that the total surfactant mass along the interface is conserved within the machine accuracy.

4 Numerical method

In this section, we present the numerical method and some related implementation details for solving the governing equations introduced in the previous section. To solve the Navier-Stokes equations (2.1)-(2.2) in a computational domain $\Omega\subset\mathbb{R}^3$, we layout a

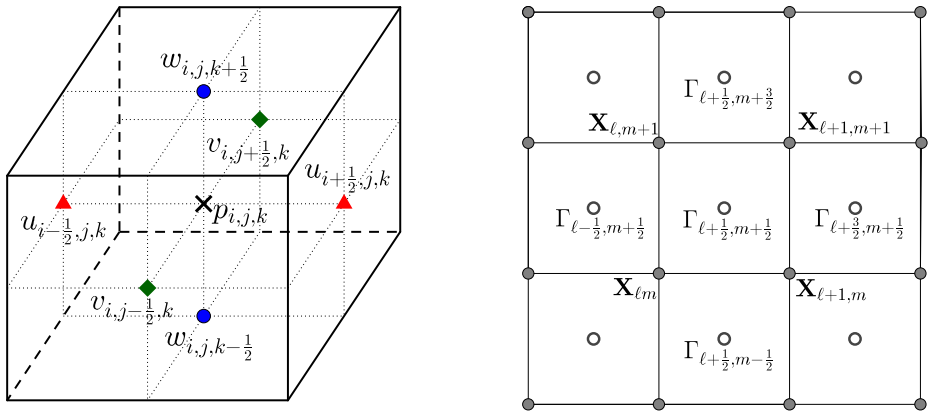

Figure 1: The left shows the locations of fluid velocities and pressure on a staggered grid in 3D. In the right, the Lagrangian markers $\mathbf{X}$ (filled circles) form a rectangular mesh and the surfactant concentration Γ (open circles) is located at the cell center of the interface.

uniform Cartesian grid with meshwidth $h=\Delta x=\Delta y=\Delta z$, and allocate the fluid velocity $\mathbf{u}=(u,v,w)$ and the pressure p in a staggered grid manner [20] as shown in the left of Fig. 1. The boundary conditions for the x and y directions are 2π periodic while the z direction is Dirichlet. As in [2], we use a Fourier representation to discretize the interface as $\mathbf{X}(\alpha,\beta,t)=(\alpha,\beta,0)^T+\mathbf{Y}(\alpha,\beta,t)$, where the first term represents the flat interface and the second term represents the periodic deviation from the plane written in truncated double Fourier series as

$$\mathbf{Y}(\alpha,\beta,t)=\sum_{k_1=-N_1/2}^{N_1/2-1}\sum_{k_2=-N_2/2}^{N_2/2-1}\widehat{\mathbf{Y}}(k_1,k_2,t)e^{i(\alpha k_1+\beta k_2)}. \tag{4.1}$$

Therefore, the interface is represented by a set of Lagrangian markers $\mathbf{X}_{\ell m}=\mathbf{X}(\alpha_\ell,\beta_m)$, where $(\alpha_\ell,\beta_m)=(\ell\Delta\alpha,m\Delta\beta)$ are the uniform grid points with the corresponding meshwidths $\Delta\alpha=2\pi/N_1$, $\Delta\beta=2\pi/N_2$ in the (α,β) plane as shown in the right of Fig. 1. The associated geometric quantities listed in previous sections such as the coefficients of the first and second fundamental forms, interface tangents and normals, and the mean curvature are all computed at the Lagrangian markers $\mathbf{X}_{\ell m}$ using the Fourier spectral differentiations [44]. These spectral derivatives with respect to α and β can be computed efficiently using Fast Fourier Transform (FFT) in a spectral accuracy. For instance, a scalar doubly periodic function $f(\alpha,\beta)$ can be written as Eq. (4.1) with the truncated Fourier coefficients $\widehat{f}(k_1,k_2)$ so the derivative with respect to α only involves the multiplication of the Fourier coefficient $\widehat{f}$ by ik_1. The inversion between the function values and its discrete Fourier coefficients can be performed efficiently using FFT. The derivative with respect to β can be computed in the same manner. To remove the aliasing error in computations, we adopt the well-known de-aliasing 2/3-rule filter [5].

4.1 A conservative scheme for solving the modified surfactant equation

As mentioned earlier, the modified surfactant equation (3.6) is in conservation form so it is quite natural to develop a conservative scheme so that the total surfactant mass along the interface is conserved. Unlike the Lagrangian markers and other geometrical quantities defined at the grid points (α_ℓ,β_m), we define the surfactant concentration at the cell center and denote it by $\Gamma_{\ell+\frac{1}{2},m+\frac{1}{2}}$ as shown in the right of Fig. 1. In the following, we discretize Eq. (3.6) using forward Euler method in time and centered difference in space as

$$\begin{aligned}
&\frac{\Gamma^{n+1}_{\ell+\frac{1}{2},m+\frac{1}{2}}(S_{\alpha\beta})^{n+1}_{\ell+\frac{1}{2},m+\frac{1}{2}}-\Gamma^{n}_{\ell+\frac{1}{2},m+\frac{1}{2}}(S_{\alpha\beta})^{n}_{\ell+\frac{1}{2},m+\frac{1}{2}}}{\Delta t}\\
&\quad-\frac{1}{\Delta\alpha}\left(\frac{(S_{\alpha\beta})^n_{\ell+1,m+\frac{1}{2}}(V_1)^{n+1}_{\ell+1,m+\frac{1}{2}}\Gamma^n_{\ell+1,m+\frac{1}{2}}}{\sqrt{E^n_{\ell+1,m+\frac{1}{2}}}}-\frac{(S_{\alpha\beta})^n_{\ell,m+\frac{1}{2}}(V_1)^{n+1}_{\ell,m+\frac{1}{2}}\Gamma^n_{\ell,m+\frac{1}{2}}}{\sqrt{E^n_{\ell,m+\frac{1}{2}}}}\right)\\
&\quad-\frac{1}{\Delta\beta}\left(\frac{(S_{\alpha\beta})^n_{\ell+\frac{1}{2},m+1}(V_2)^{n+1}_{\ell+\frac{1}{2},m+1}\Gamma^n_{\ell+\frac{1}{2},m+1}}{\sqrt{G^n_{\ell+\frac{1}{2},m+1}}}-\frac{(S_{\alpha\beta})^n_{\ell+\frac{1}{2},m}(V_2)^{n+1}_{\ell+\frac{1}{2},m}\Gamma^n_{\ell+\frac{1}{2},m}}{\sqrt{G^n_{\ell+\frac{1}{2},m}}}\right)\\
&=\frac{1}{Pe_s\Delta\alpha}\left[\frac{1}{(S_{\alpha\beta})^n_{\ell+1,m+\frac{1}{2}}}\left(G^n_{\ell+1,m+\frac{1}{2}}\frac{\Gamma^n_{\ell+\frac{3}{2},m+\frac{1}{2}}-\Gamma^n_{\ell+\frac{1}{2},m+\frac{1}{2}}}{\Delta\alpha}-F^n_{\ell+1,m+\frac{1}{2}}\frac{\Gamma^n_{\ell+1,m+1}-\Gamma^n_{\ell+1,m}}{\Delta\beta}\right)\right.\\
&\quad\left.-\frac{1}{(S_{\alpha\beta})^n_{\ell,m+\frac{1}{2}}}\left(G^n_{\ell,m+\frac{1}{2}}\frac{\Gamma^n_{\ell+\frac{1}{2},m+\frac{1}{2}}-\Gamma^n_{\ell-\frac{1}{2},m+\frac{1}{2}}}{\Delta\alpha}-F^n_{\ell,m+\frac{1}{2}}\frac{\Gamma^n_{\ell,m+1}-\Gamma^n_{\ell m}}{\Delta\beta}\right)\right]\\
&\quad+\frac{1}{Pe_s\Delta\beta}\left[\frac{1}{(S_{\alpha\beta})^n_{\ell+\frac{1}{2},m+1}}\left(E^n_{\ell+\frac{1}{2},m+1}\frac{\Gamma^n_{\ell+\frac{1}{2},m+\frac{3}{2}}-\Gamma^n_{\ell+\frac{1}{2},m+\frac{1}{2}}}{\Delta\beta}-F^n_{\ell+\frac{1}{2},m+1}\frac{\Gamma^n_{\ell+1,m+1}-\Gamma^n_{\ell,m+1}}{\Delta\alpha}\right)\right.\\
&\quad\left.-\frac{1}{(S_{\alpha\beta})^n_{\ell+\frac{1}{2},m}}\left(E^n_{\ell+\frac{1}{2},m}\frac{\Gamma^n_{\ell+\frac{1}{2},m+\frac{1}{2}}-\Gamma^n_{\ell+\frac{1}{2},m-\frac{1}{2}}}{\Delta\beta}-F^n_{\ell+\frac{1}{2},m}\frac{\Gamma^n_{\ell+1,m}-\Gamma^n_{\ell m}}{\Delta\alpha}\right)\right],
\end{aligned}\tag{4.2}$$

where $S_{\alpha\beta}$ denotes $|\mathbf{X}_\alpha\times\mathbf{X}_\beta|=\sqrt{EG-F^2}$, the local stretching factor on the interface. In the above scheme, all the variables except Γ are defined at the Lagrangian marker $\mathbf{X}$ shown in Fig. 1. So, when a variable is necessarily shifted by a half-mesh width for relevant computations, the linear interpolation is simply employed. For instance, we define

$$(S_{\alpha\beta})^n_{\ell+\frac{1}{2},m}=\frac{(S_{\alpha\beta})^n_{\ell m}+(S_{\alpha\beta})^n_{\ell+1,m}}{2}$$

and

$$(S_{\alpha\beta})^n_{\ell+\frac{1}{2},m+\frac{1}{2}}=\frac{(S_{\alpha\beta})^n_{\ell m}+(S_{\alpha\beta})^n_{\ell+1,m}+(S_{\alpha\beta})^n_{\ell,m+1}+(S_{\alpha\beta})^n_{\ell+1,m+1}}{4}.$$

In the similar fashion, the surfactant concentration $\Gamma^n_{\ell m}$ can be linearly interpolated from the values of neighboring four points.

By taking the double summation with respect to ℓ and m on both sides of Eq. (4.2) and using the doubly periodic boundary condition, one can easily prove that the total surfactant mass in the scheme (4.2) is conserved. That is,

$$\sum_{\ell=0}^{N_1-1}\sum_{m=0}^{N_2-1}\Gamma^{n+1}_{\ell+\frac{1}{2},m+\frac{1}{2}}(S_{\alpha\beta})^{n+1}_{\ell+\frac{1}{2},m+\frac{1}{2}}\Delta\alpha\Delta\beta=\sum_{\ell=0}^{N_1-1}\sum_{m=0}^{N_2-1}\Gamma^{n}_{\ell+\frac{1}{2},m+\frac{1}{2}}(S_{\alpha\beta})^{n}_{\ell+\frac{1}{2},m+\frac{1}{2}}\Delta\alpha\Delta\beta. \tag{4.3}$$

Notice that, this conservation property in Eq. (4.2) is independent of the numerical scheme for computing the quantities associated with the interfacial geometry and the artificial tangential velocity such as $E,F,G,S_{\alpha\beta}$ and V_1,V_2, respectively. In the next section, the relative error of total surfactant mass versus time will be presented to verify the mass conservation for various numerical experiments.

4.2 Time-stepping scheme

We here present how to march the Lagrangian markers $\mathbf{X}^n=\mathbf{X}(n\Delta t)$ from time level n to obtain $\mathbf{X}^{n+1}=\mathbf{X}(n\Delta t+\Delta t)$ at time level $n+1$ with Δt the time step size. In the present IB method, the surfactant concentration Γ^n, the fluid velocity $\mathbf{u}^n$, the pressure p^n, and the Lagrangian markers $\mathbf{X}^n$ are all given in advance, and from these variables we aim to update Γ^{n+1}, $\mathbf{u}^{n+1}$, p^{n+1}, and $\mathbf{X}^{n+1}$. The step-by-step numerical procedure can be done as follows.

1. At the Lagrangian markers $\mathbf{X}^n_{\ell m}$, we first compute the tension by $\sigma_{\ell m}=\sigma(\mathbf{X}^n_{\ell m})=\sigma_0(1-\eta\Gamma^n_{\ell m})$, and then compute the interfacial tension force

$$\mathbf{F}(\mathbf{X}^n_{\ell m})\mathrm{d}A(\mathbf{X}^n_{\ell m})=(\nabla_s\sigma_{\ell m}-2\sigma_{\ell m}H_{\ell m}\mathbf{n}_{\ell m})\mathrm{d}A(\mathbf{X}^n_{\ell m}),$$

   where the (tangential) Marangoni force density $\nabla_s\sigma_{\ell m}$ and the (normal) capillary force density $2\sigma_{\ell m}H_{\ell m}\mathbf{n}_{\ell m}$ are obtained using the formulas written in earlier sections. The surface area element is computed by $\mathrm{d}A(\mathbf{X}^n_{\ell m})=(S_{\alpha\beta})^n_{\ell m}\Delta\alpha\Delta\beta$.

2. Distribute the tension force acting on Lagrangian markers into the Eulerian grid by using the smoothed Dirac delta function δ_h as

$$\mathbf{f}^n(\mathbf{x})=\sum_{\ell=0}^{N_1-1}\sum_{m=0}^{N_2-1}\mathbf{F}(\mathbf{X}^n_{\ell m})\delta_h(\mathbf{x}-\mathbf{X}^n_{\ell m})\mathrm{d}A(\mathbf{X}^n_{\ell m}), \tag{4.4}$$

   where $\mathbf{x}=(x,y,z)$ is the Eulerian grid point. For $\delta_h(\mathbf{x})=\frac{1}{h^3}\phi\left(\frac{x}{h}\right)\phi\left(\frac{y}{h}\right)\phi\left(\frac{z}{h}\right)$, we employ the 4-point supported function ϕ developed in [50] to suppress spurious force oscillations in IB method.

3. Solve the Navier-Stokes equations by the second-order incremental pressure-correction projection method in [18] as follows.

$$\begin{aligned}
&\frac{3\mathbf{u}^\star-4\mathbf{u}^n+\mathbf{u}^{n-1}}{2\Delta t}+2(\mathbf{u}^n\cdot\nabla_h)\mathbf{u}^n-\left(\mathbf{u}^{n-1}\cdot\nabla_h\right)\mathbf{u}^{n-1}\\
&=-\nabla_h p^n+\frac{1}{Re}\left[\lambda\Delta\mathbf{u}^\star-\lambda\Delta\mathbf{u}^n+\nabla_h\cdot\left(\mu\left(\nabla_h\mathbf{u}^n+(\nabla_h\mathbf{u}^n)^T\right)\right)\right]+\frac{\mathbf{f}^n}{ReCa},\\
&\Delta_h p^\star=\frac{3}{2\Delta t}\nabla_h\cdot\mathbf{u}^\star,\qquad \frac{\partial p^\star}{\partial\mathbf{n}}=0\ \text{ on }\partial\Omega_D,\qquad \mathbf{u}^\star=\mathbf{u}^{n+1}\ \text{ on }\partial\Omega_D,\\
&\mathbf{u}^{n+1}=\mathbf{u}^\star-\frac{2\Delta t}{3}\nabla_h p^\star,\qquad \nabla_h p^{n+1}=\nabla_h p^\star+\nabla_h p^n-\frac{2\lambda\Delta t}{3Re}\Delta_h(\nabla_h p^\star),
\end{aligned}$$

where the discrete operators ∇_h and $\nabla_h\cdot$ approximate the gradient and divergence operators, respectively, using the second-order finite difference in staggered grid. For the nonlinear terms, the skew-symmetric form is employed as $(\mathbf{u}\cdot\nabla_h)\mathbf{u}=\frac{1}{2}(\mathbf{u}\cdot\nabla_h)\mathbf{u}+\frac{1}{2}\nabla_h(\mathbf{uu})$. The domain boundary is denoted by $\partial\Omega_D$. Here, $\lambda=\mu^-/\mu^+$ is the viscosity contrast while the dimensionless viscosity can be defined by $\mu=1+(\lambda-1)I(\mathbf{x})$ after the normalization using μ^+. The indicator function $I(\mathbf{x})=1$ in Ω^- and zero elsewhere can be obtained by solving Poisson equation as described in [45].

4. Once $\mathbf{u}^{n+1}$ is determined in the Eulerian fluid points, we interpolate the fluid interfacial velocity $\mathbf{U}_{\ell m}^{n+1}=\sum_{\mathbf{x}}\mathbf{u}^{n+1}(\mathbf{x})\delta_h(\mathbf{x}-\mathbf{X}_{\ell m}^n)h^3$ in Eq. (3.1). In order to maintain an equi-arclength distribution of updated Lagrangian markers, it requires to solve the artificial velocities $(V_1)_{\ell m}^{n+1}$ and $(V_2)_{\ell m}^{n+1}$ in Eqs. (3.4) and (3.5), respectively. This can be simply done using the fixed point iteration by taking $V_2=0$ initially. The error of tolerance is set to be $h/100$ so that only 2-3 iterations are needed in each time step. (Note that, the magnitude of the error of tolerance affects only the accuracy of V_1 and V_2 here. Since the immersed boundary method is first-order accurate in general, as long as we choose the error of tolerance as the same order of the method accuracy, it has no significant effect on the surfactant and fluid variables as a whole.) For the numerical integration in (3.4) and (3.5), the trapezoidal rule is used. Therefore, the new Lagrangian markers can be updated by

$$\mathbf{X}_{\ell m}^{n+1}=\mathbf{X}_{\ell m}^n+\Delta t\left(\mathbf{U}_{\ell m}^{n+1}+(V_1)_{\ell m}^{n+1}\left(\boldsymbol{\tau}^1\right)_{\ell m}^n+(V_2)_{\ell m}^{n+1}\left(\boldsymbol{\tau}^2\right)_{\ell m}^n\right).$$

5. After computing $(S_{\alpha\beta})_{\ell+\frac{1}{2},m+\frac{1}{2}}^{n+1}$, we update surfactant concentration distribution $\Gamma_{\ell+\frac{1}{2},m+\frac{1}{2}}^{n+1}$ using Eq. (4.2), and then apply the linear interpolation to obtain $\Gamma_{\ell m}^{n+1}$.

We summarize the implementing difficulties and differences for the numerical algorithm between previous 2D [25,26] and the present 3D version as follows. Besides the computational complexity of the fluid solver used, the significant differences fall into the

handling of the interface (an evolving curve in 2D and an evolving surface in 3D) and solving the surfactant equation on the corresponding interfaces. As discussed in Section 3, to keep the interface mesh as equi-arclength distributed, two artificial tangential velocity components must be determined in 3D rather than one component in 2D. The modified surfactant equation in 3D involves solving convection-diffusion equation on an evolving surface which is much more difficult to solve than in 2D case as we have emphasized in the third paragraph of the Introduction. Here, we develop an explicit scheme for the modified surfactant equation being able to save the computational cost and to preserve the total surfactant mass exactly.

5 Numerical results

A series of numerical experiments is carried out in this section. Firstly, we examine the effect and necessity of the equi-arclength Lagrangian mesh control developed in Section 3. We then check the rates of convergence for the velocity field, interfacial configuration, and the surfactant concentration. Self-healing dynamics in quiescent flow with non-unity viscosity contrast is investigated in detail and show qualitatively similar results with the ones obtained in literature. Lastly, we study the two-layer fluids under Couette flow with different physical parameters in detail. Throughout the paper, the velocity boundary conditions in both x and y directions are set to be 2π periodic while in the z direction is Dirichlet. Since the interface is parallel to $x-y$ plane initially, the interface is also 2π doubly periodic as described in the beginning of Section 4.

5.1 Effect of Lagrangian mesh control

As mentioned earlier, for a deforming surface with interfacial tension in fluid flows, the underlying Lagrangian mesh will inevitably distort and consequently induce numerical instability of computations. In this subsection, we check the performance and necessity of the enforcement of the equi-arclength parametrization mesh control technique presented in Section 3. The problem setup is the following. We assume the interface is flat initially in the plane $z=\pi$ with the initial surfactant concentration

$$\Gamma(\alpha,\beta,0)=\frac{1-\tanh(20(2-r))}{2}, \tag{5.1}$$

where r is the distance of Lagrangian marker from the center (π,π,π). So the centered region is almost surfactant free $\Gamma\approx 0$, while the outside region is $\Gamma\approx 1$, see Fig. 2(a) in detail. The flow is quiescent so the only driving force to the fluid comes from the surface tension. We also choose the same viscosity for the upper and lower fluids; that is, the viscosity contrast $\lambda=\mu^-/\mu^+=1$. In this test, we use $Re=1$, $Ca=0.01$, $Pe_s=1$, and $\eta=0.8$. We fix $\sigma_0=1$ for all tests carried out in this paper. The grid size is 128^3 in the computational domain $[0,2\pi]^3$ so the fluid mesh width is $h=2\pi/128$. The number of

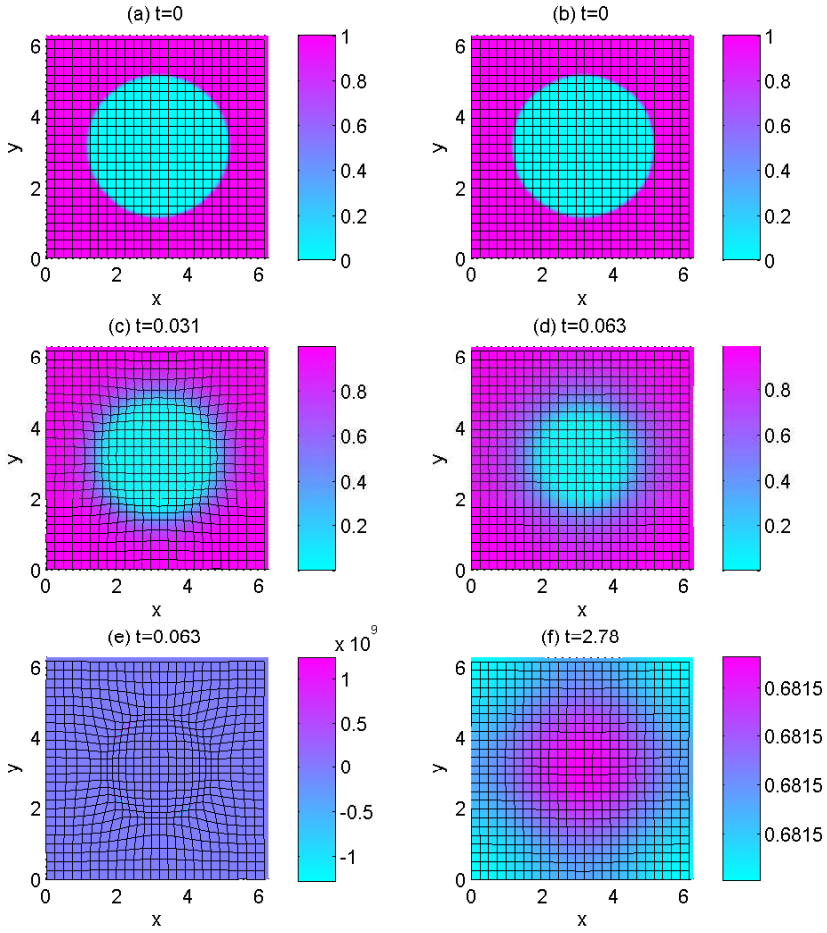

Figure 2: The underlying Lagrangian mesh and the corresponding surfactant concentration at different times. Left panel (without mesh control); right panel (with mesh control).

Lagrangian markers on the interface is 256^2 so the Lagrangian mesh is $\Delta\alpha = \Delta\beta = h/2$. The time step size is chosen as $\Delta t = h/512$.

Since the interface is flat and 2π doubly periodic, the only mechanism driving the fluid dynamics is the inward Marangoni force due to surface tension gradient (thus surfactant concentration gradient). Fig. 2 shows the underlying Lagrangian mesh and the corresponding surfactant concentration at different times in which the left panel is the one without imposing equi-arclength mesh control while the right panel is the one with mesh control. One can immediately see from Fig. 2(c) and (e) that the grid lines distort significantly and eventually the computation breaks down at $t = 0.063$, see the erroneous value scale. However, for the results with mesh control in Fig. 2(d) and (f), the Lagrangian mesh remains uniformly and the surfactant undergoes uniform spreading on the flat interface.

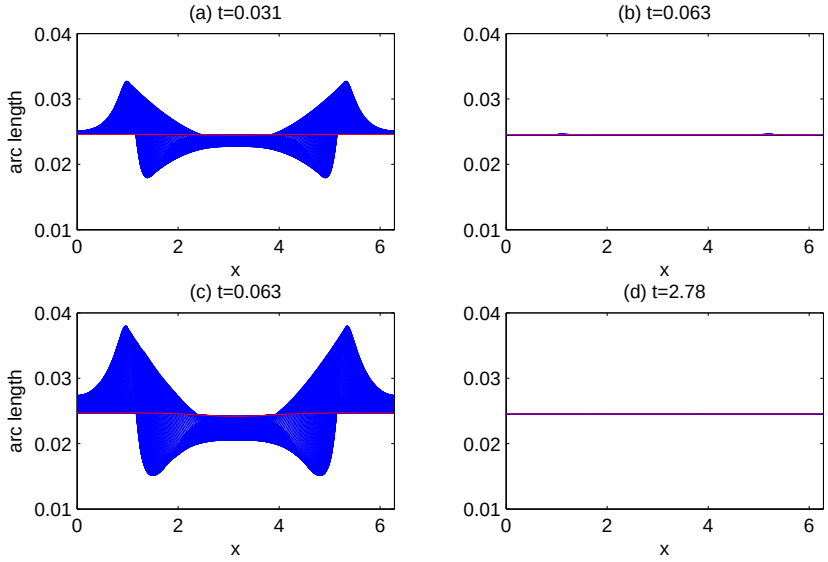

Figure 3: The plots of arclength $|\mathbf{X}_\alpha|\Delta\alpha$. (a)-(d) correspond to Fig. 2(c)-(f), respectively. The straight red line is the initial uniform arclength.

Fig. 3 shows the corresponding plots of the arclength $|\mathbf{X}_\alpha|\Delta\alpha$ for each α-directed curve at some selected times, in which (a)-(d) correspond to Fig. 2(c)-(f). We can clearly see that the arclength in the vicinity of the circular border of surfactant-free region varies considerably and its deviation becomes significant as time evolves as shown in Fig. 3(a) and (c), while the arclength is a nearly constant (overlapped with solid red lines) in Fig. 3(b) and (d).

Fig. 4(a) depicts the fluid velocity field (u,v) on the plane $z=\pi$ corresponding to Fig. 2(d) which indeed shows the Marangoni force driving the fluid motion inwardly. Fig. 4(b) depicts the velocity (u,w) on the plane $y=\pi$ in which one can see the circulatory motion appears. The corresponding streamline of Fig. 4(b) is shown in (c) to demonstrate the interface keeps flat as initially so no penetration flow occurs (normal velocity approximates to zero numerically). Fig. 4(c) also shows that the fluid leakage across the interface is negligible as long as the number of Lagrangian markers and the time step size are chosen appropriately.

5.2 Convergence study

In this subsection, we perform a convergence study of the present numerical method with respect to fluid velocity, Lagrangian marker, and surfactant concentration. The dimensionless parameters are also chosen by $Re=1$, $Ca=0.01$, $Pe_s=1$, and $\eta=0.8$. The viscosity contrast is set by $\lambda=2$, which will consequently lead to interface deformation. We set the time step size by $\Delta t=h/256$. For the computational domain $[0,2\pi]^3$, we use

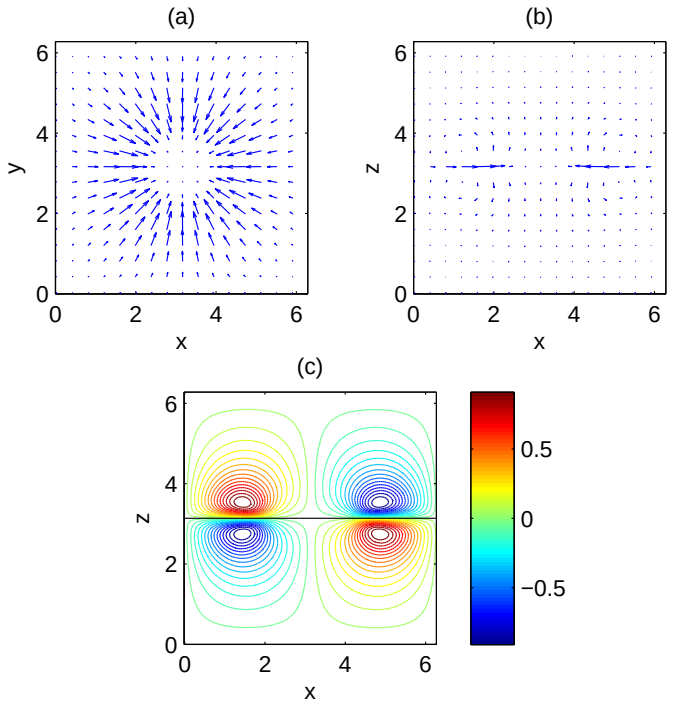

Figure 4: At $t=0.063$ with mesh control corresponding to Fig. 2(d). (a) the velocity field on the plane $z=\pi$; (b) the velocity field on the plane $y=\pi$; (c) the circulatory streamline corresponding to (b) with the flat interface at $z=\pi$. The color represents the stream function magnitude.

four different Cartesian grid sizes $N=32,64,128,256$ to estimate the convergence rate of the variables. In the interface discretization, as we double the grid size N, we increase the number of Lagrangian markers by a factor of four accordingly. As previous example, the initial interface is a flat plane and the initial distribution of surfactant is given by $\Gamma(\alpha,\beta,0)=(1-\tanh(20(2-r)))/2$, where r is defined as in previous example. The resultant motion up to $t=2.4$ are similar to the inward spreading of surfactant illustrated in Figs. 6 and 7(a).

Table 1 exhibits the rates of convergence of the velocity components $\mathbf{u}=(u,v,w)$, the interfacial marker $\mathbf{X}$, and the surfactant concentration Γ at two different times $t=1.5$ and $t=2.4$, respectively. In this test, the analytic solution is not known, so we compute the convergence rate by estimating the two successive errors as

$$\text{Rate}=\log_2(\|u_N-u_{2N}\|_\infty/\|u_{2N}-u_{4N}\|_\infty).$$

The error $\|u_N-u_{2N}\|_\infty$ is the maximum absolute difference of the numerical solutions for the grid N and the grid $2N$. The rates for other variables are defined in a similar manner. One can see from Table 1 that the average rate is around one for all variables indicating that our numerical scheme is roughly first-order accurate. This supports that the IB method is generally first-order accurate.

Table 1: Convergence rates of the fluid velocity $\mathbf{u}=(u,v,w)$, the Lagrangian markers $\mathbf{X}$, and the surfactant concentration Γ at time $t=1.5$ and 2.4.

N	$\|u_N-u_{2N}\|_\infty$	Rate	$\|v_N-v_{2N}\|_\infty$	Rate	$\|w_N-w_{2N}\|_\infty$	Rate
$t=1.5$						
32	5.112E-02	-	5.734E-02	-	4.694E-02	-
64	2.463E-02	1.05	2.758E-02	1.06	1.933E-02	1.28
128	1.181E-02	1.06	1.287E-02	1.10	8.954E-03	1.11
$t=2.4$						
32	3.302E-02	-	3.472E-02	-	2.109E-02	-
64	1.219E-02	1.44	1.300E-02	1.42	8.910E-03	1.24
128	5.792E-03	1.07	5.981E-03	1.12	4.433E-03	1.01
N	$\|\mathbf{X}_N-\mathbf{X}_{2N}\|_\infty$	Rate	$\|\Gamma_N-\Gamma_{2N}\|_\infty$	Rate		
$t=1.5$						
32	9.935E-02	-	1.601E-02	-		
64	5.581E-02	0.83	5.973E-03	1.42		
128	2.863E-02	0.96	2.635E-03	1.18		
$t=2.4$						
32	1.061E-01	-	1.028E-02	-		
64	5.654E-02	0.91	3.674E-03	1.48		
128	2.875E-02	0.98	1.559E-03	1.24		

Fig. 5(a) shows the time evolutional plots for maximum amplitude of the interface in the z-direction for four cases of $N=32,64,128$, and 256. Throughout this paper, the maximum amplitude of the interface indicates the difference between the highest and lowest position coordinates in z-direction. Obviously the maximum amplitude profile has a tendency to converge as the grid number increases. In Fig. 5(b), the relative error of

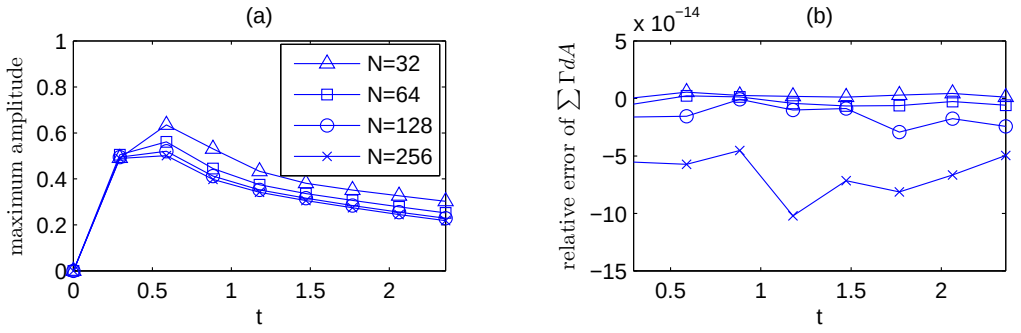

Figure 5: (a) The maximum amplitude of the deforming interface in the z-direction; (b) the relative error of total surfactant mass.

total surfactant mass $\sum\Gamma \mathrm{d}A$ is shown for all cases to verify the exact conservation of the total mass. Here, the relative error at time level n is defined by

$$\text{error} = \left(\sum_{\ell,m} \Gamma^n_{\ell+\frac{1}{2},m+\frac{1}{2}} (S_{\alpha\beta})^n_{\ell+\frac{1}{2},m+\frac{1}{2}} \Big/ \sum_{\ell,m} \Gamma^0_{\ell+\frac{1}{2},m+\frac{1}{2}} (S_{\alpha\beta})^0_{\ell+\frac{1}{2},m+\frac{1}{2}} \right) - 1 \tag{5.2}$$

referring to Eq. (4.3). One can see that the relative error is within machine accuracy which indicates that our scheme preserves the total surfactant mass exactly.

5.3 Self-healing dynamics

In this subsection, we study the self-healing motion [42] for a deforming interface driven by surfactant spreading inwardly and outwardly in quiescent flow. For all runs, the stresses on the interfacial fluid are generated by surfactant concentration gradients, thus the surrounding fluid moves inducing the surfactant transport. The inward and outward spreadings are dependent on the initial condition of surfactant distribution. In order to obtain similar qualitative results observed in [42], we here choose parameters $Ca = 0.1$, $Pe_s = 1000$, and $\eta = 0.5$. The Reynolds number is chosen by $Re = 10^{-5}$ to be in Stokes regime. The viscosity contrast is $\lambda = 2$, where the lower layer fluid is slightly more viscous than the upper one. The fluid mesh size is 128^3 in the computational domain $[0,2\pi]^3$.

5.3.1 Inward spreading of surfactant

We study the interfacial deformation due to inward spreading of surfactant whose initial concentration on a flat interface located at $z = \pi/10$ is $\Gamma = (1-\tanh(20(1.8-r)))/2$ as shown in Fig. 6(a). When $t = 0$, the surfactant exists outside the circle with radius 1.8 measured from the interfacial center and, as time evolves, it spreads inwards. As observed in Fig. 6(b), an annular ridge is developed as the interfacial fluid is pulled by the surfactant transport into the clean inner region. The fluid ridge then deforms into a single peaked shape in Fig. 6(c), and eventually the interface undergoes a relaxation as depicted in Fig. 6(d). The color on the deforming interface indicates the surfactant concentration Γ showing its maximum and minimum at the color-bar. It is worth mentioning that the present results in Fig. 6 show a good preservation of the symmetric structure during the simulation.

In Fig. 7(a), some sectional views at $y=\pi$ of the interfacial profile at different times are plotted. As discussed above, the initial flat interface is deformed to the annular ridge, and then this structure coalesces into a central peak. The corresponding distributions of surfactant concentration are shown in Fig. 7(b) in which the surfactant-free region becomes narrower as time evolves. Fig. 7(c) shows the time evolutional plot of the maximum amplitude of the deforming interface which shows the relaxation of interface. Fig. 7(d) shows the relative error of total surfactant mass during the time evolution. Once again, the total surfactant mass conservation is confirmed.

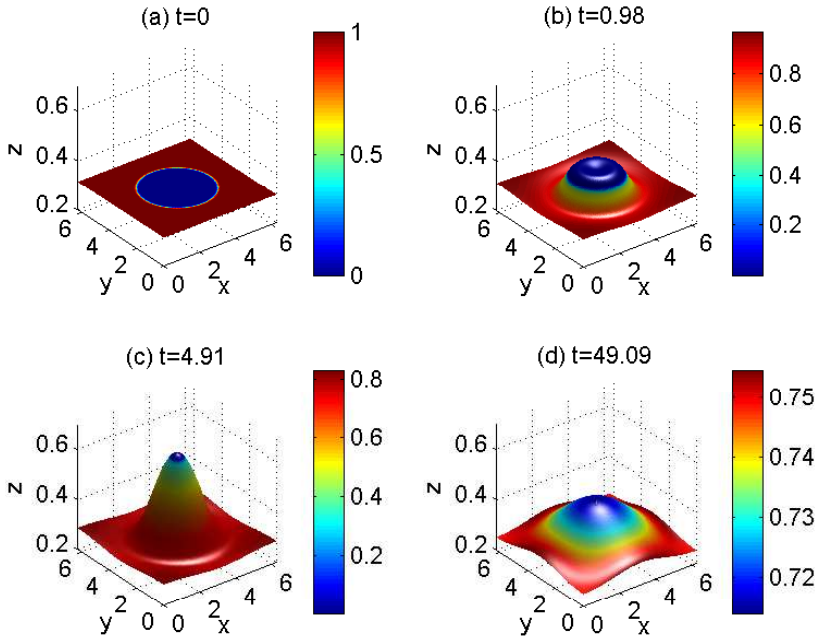

Figure 6: Interfacial deformations due to inward spreading of surfactant at different times. The color represents the surfactant concentration Γ.

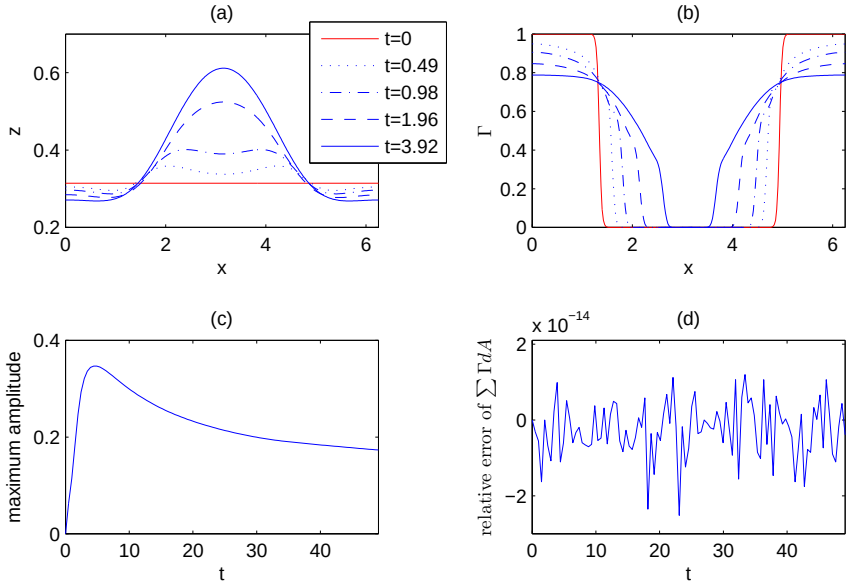

Figure 7: Inward spreading of surfactant. (a) the sectional view of evolving interface at $y=\pi$; (b) the corresponding surfactant concentration Γ on those curves in (a); (c) the time evolutional plot of the maximum amplitude of the deforming interface in the z-direction; (d) the relative error of total surfactant mass.

In our results of this inward spreading dynamics, the evolution of the interface and surfactant distribution are quite qualitatively comparable to that of observed using different equation of state in [39], although we use the linear equation of state (2.5). There is another difference that we solve the Navier-Stokes equations while the authors in [39] solve a modified thin film equation. Further studies in the future are needed for better understanding of this physical phenomenon.

5.3.2 Outward spreading of surfactant

We next study the interfacial deformation due to outward spreading of surfactant whose initial concentration on a flat interface located at $z=\pi/10$ is $\Gamma=(1+\tanh(20(1.8-r)))/2$ shown in Fig. 8(a). Unlike the previous one, the surfactant now is initially confined in the circle with radius 1.8 and then spreads outwards. In Fig. 8(b), an outward-spreading annular ridge is observed as the interfacial fluid is pushed by the surfactant transport into the outer clean region. In contrast to inward spreading, the fluid ridge is not coalesced into a single central peaked shape but maintains the ridge structure for quite a long time as shown in Fig. 8(c). As in previous case, Fig. 9(a)-(d) show the sectional view of evolving interface at $y=\pi$, the corresponding surfactant concentration Γ, the time evolutional plot of the maximum amplitude of the deforming interface in the z-direction, and the relative error of total surfactant mass, respectively. One can see in Fig. 9(b), the surfactant

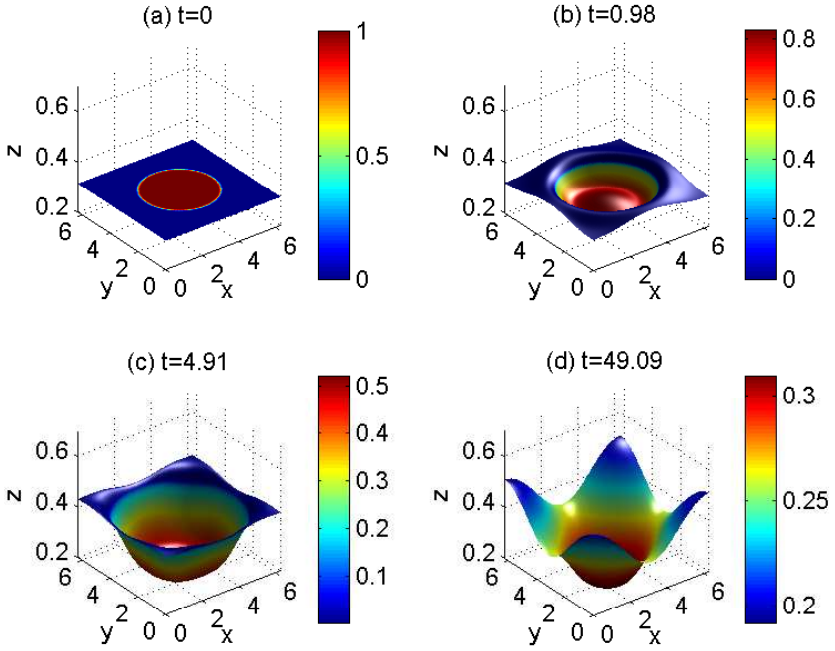

Figure 8: Interfacial deformations due to outward spreading of surfactant at different times. The color represents the surfactant concentration Γ.

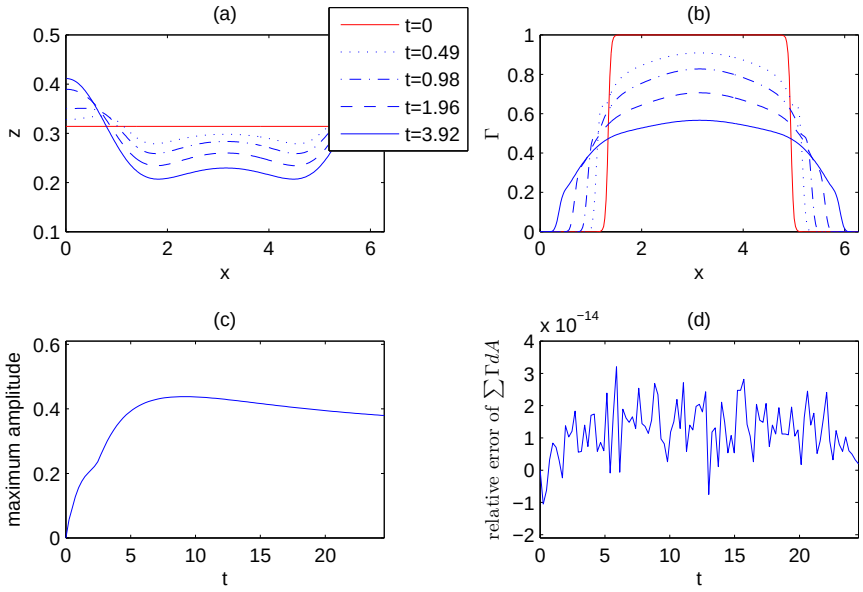

Figure 9: Outward spreading of surfactant. (a) the sectional view of evolving interface at $y=\pi$; (b) the corresponding surfactant concentration Γ on those curves in (a); (c) the time evolutional plot of the maximum amplitude of the deforming interface in the z-direction; (d) the relative error of total surfactant mass.

indeed spreads outwardly as time evolves. In Fig. 9(c), the maximum amplitude of the interface shows a slow decay of the fluid ridge and this decay rate is smaller than that of inward spreading shown in Fig. 7(c). This result is also qualitatively comparable with the one found in [39]. The relative error of total surfactant mass shown in Fig. 9(d) is still within the machine accuracy.

5.4 Two-layer fluids in Couette flow

In order to further validate our present method, we simulate the dynamics of two-layer fluids in Couette flow with surfactant. With the presence of insoluble surfactant along the interface, the resultant dynamics generate complex interfacial behaviors such as wave propagation of the interface. A recent review on this thin film problem can be found in [8]. As shown in Figs. 11(a) and 12(a), the initial layer is perturbed from a flat plane by finite amplitude sinusoidal waves as $\mathbf{X}=\big(\alpha,\beta,2\pi/10+0.1\sum_{k=1}^{3}(\sin k\alpha\sin k\beta)\big)$ in $[0,2\pi]^3$. To impose a Couette flow, the Dirichlet boundary condition of $\mathbf{u}=(z,0,0)$ is enforced only in the z-direction while other boundary conditions remain fully periodic. The initial surfactant concentration is uniformly distributed by $\Gamma=0.5$. In this simulation, we aim to investigate the surfactant effect (with or without surfactant) on the maximum amplitude of the interface when the capillary number Ca varies. The other parameters are set by $Pe_s=1000$, $Re=1$, $\lambda=4$, and $\Delta t=h/32$. All numerical results are obtained up to time $t=50$.

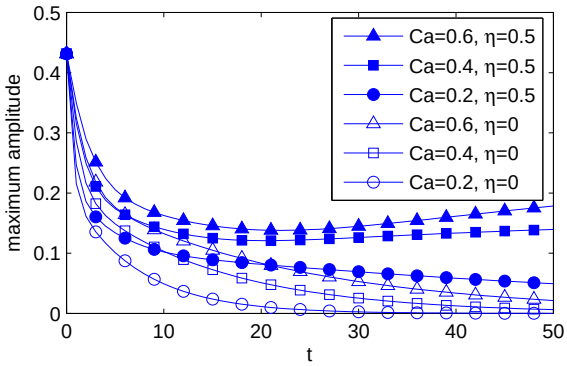

Figure 10: Two-layer fluids in Couette flow. The time evolutional plots of the interface maximum amplitudes for different capillary numbers $Ca=0.2,0.4,0.6$. The parameter $\eta=0$ represents the case of without surfactant while $\eta=0.5$ represents the one with surfactant.

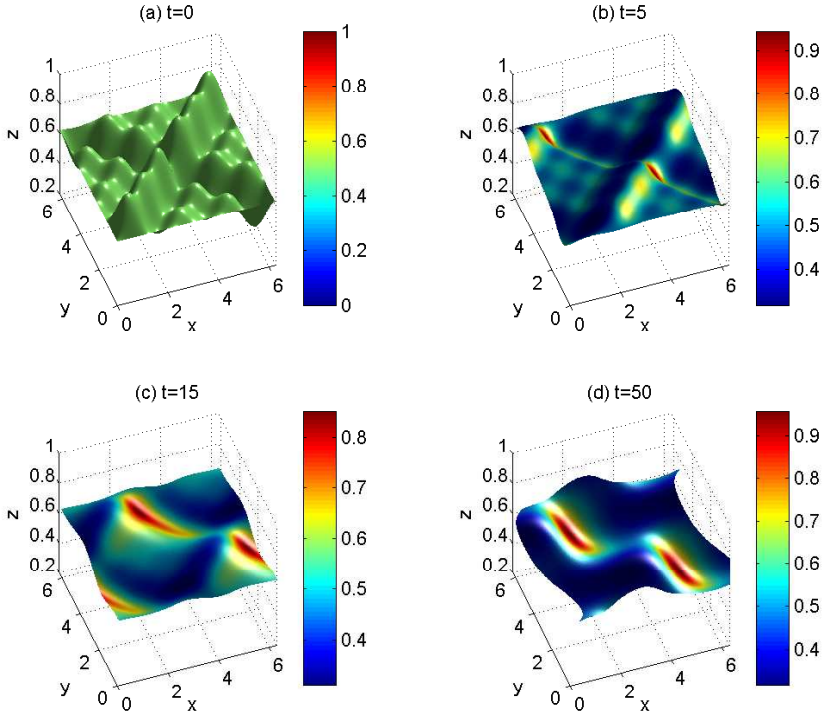

Figure 11: In the presence of surfactant ($\eta=0.5, Ca=0.6$), the initially perturbed interface under Couette flow tends to amplify and develops into a wavy surface. The color represents the surfactant concentration Γ.

We vary Ca from 0.2 to 0.6 to study how the different capillary number affects the interfacial deformation. Fig. 10 shows the time evolutionary plot of the maximum amplitude of the interface for different capillary numbers. One can see that, in the beginning, all the maximum amplitudes tend to decrease significantly, but for the ones with

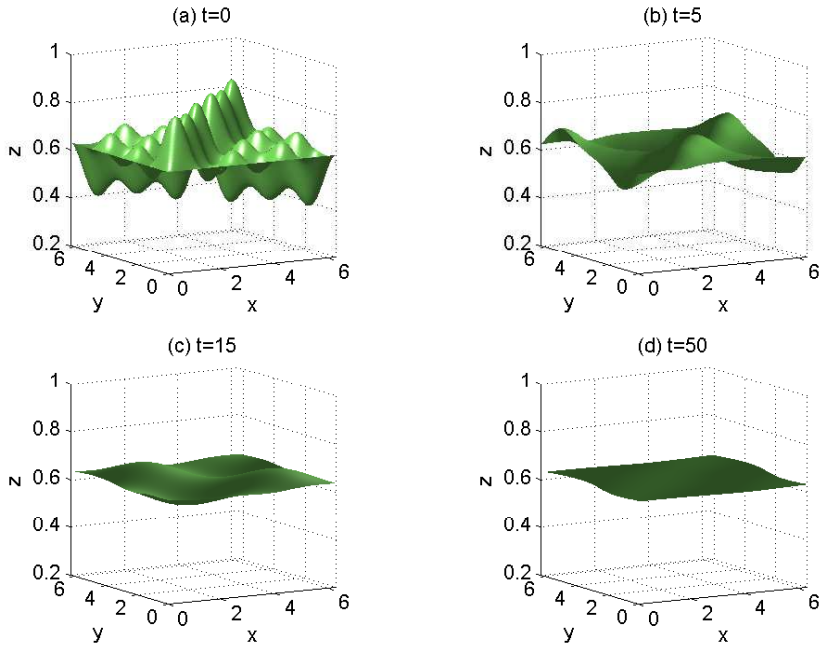

Figure 12: In the absence of surfactant ($\eta=0, Ca=0.6$), the initially perturbed interface under Couette flow tends to damp out and becomes a flat surface eventually.

surfactant ($\eta=0.5$) and higher capillary number ($Ca=0.4,0.6$), the maximum amplitude increases at some time indicating an unstable interface occurs. For the case $\eta=0.5$ and $Ca=0.2$, the maximum amplitude keeps decreasing just like the ones without surfactant ($\eta=0$). Fig. 11 shows the interface profile and the corresponding surfactant concentration at different times for the case of $\eta=0.5$ and $Ca=0.6$, while Fig. 12 shows the interface profile for the case of $\eta=0$ and $Ca=0.6$. One can clearly see that without the surfactant, the finite interfacial perturbation tends to damp out eventually, while with the surfactant, the interface amplitude amplifies. Furthermore, during the time evolution, a wavy interface appears in both cases as we can see from Fig. 13(a) and (b) which are the sectional views of the interfaces for Fig. 11 and Fig. 12, respectively. Thus, we can conclude that the surfactant indeed plays an important role in the interfacial stability under Couette flow.

6 Conclusions and future work

In this paper, we have proposed a three-dimensional immersed boundary method for interfacial flows with insoluble surfactant. We enforce an equi-arclength parametrization on the interface by adding two artificial tangential velocity to the Lagrangian marker velocity so that the surface Lagrangian mesh can be uniformly distributed in numerical computations without any re-meshing. With this mesh-control technique, the computa-

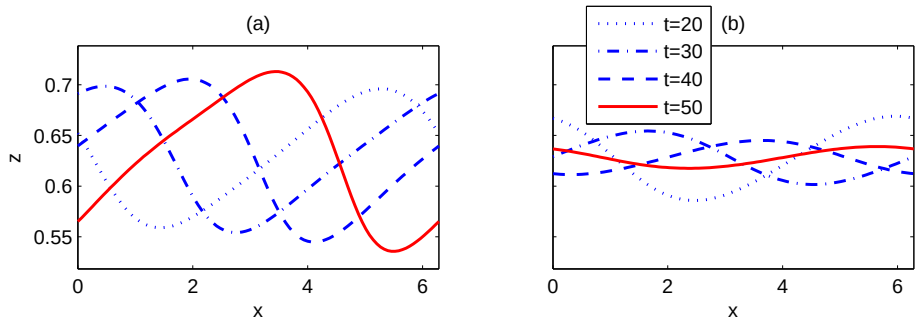

Figure 13: The sectional views of interface with fixed $y=\pi/2$ at different times. (a) and (b) correspond to Figs. 11 and 12, respectively.

tions are stable up to long time simulations. Meanwhile, under this new parametrization, the surfactant concentration equation is modified accordingly. And we develop a conservative scheme to solve the modified surfactant equation so that the total surfactant mass is conserved numerically. We have performed a series of numerical tests to validate our present scheme. In the future, we plan to extend our current method to handle the case of compact interfaces such as a droplet, and to the soluble surfactant case as well.

Acknowledgments

The work of M.-C. Lai was supported in part by Ministry of Science and Technology of Taiwan under research grant MOST-104-2115-M-009-014-MY3 and NCTS. We also like to thank Dr. Te-sheng Lin for his helpful discussions.

References

[1] S. Adami, X.Y. Hu, N.A. Adams, A conservative SPH method for surfactant dynamics, J. Comput. Phys., 229 (2010) 1909-1926.
[2] D.M. Ambrose, M. Siegel, S. Tlupova, A small-scale decomposition for 3D boundary integral computations with surface tension, J. Comput. Phys., 247 (2013), 168-191.
[3] J.W. Barrett, H. Garcke, R. Nürnberg, Stable finite element approximations of two-phase flow with soluble surfactant, J. Comput. Phys., 297 (2015), 530-564.
[4] I.B. Bazhlekov, P.D. Anderson, H.E.H. Meijer, Numerical investigation of the effect of insoluble surfactants on drop deformation and breakup in simple shear flow, J. Colloid Interface Sci., 298 (2006), 369-394.
[5] C. Canuto, M.Y. Hussaini, A. Quarteroni, T.A. Zang, Spectral Methods in Fluid Dynamics, Springer-Verlag, 1988.
[6] H.D. Ceniceros, The effects of surfactants on the formation and evolution of capillary waves, Phys. Fluids, 15 (2003), 245-256.
[7] K.-Y. Chen, M.-C. Lai, A conservative scheme for solving coupled surface-bulk convection-diffusion equations with an application to interfacial flows with soluble surfactant, J. Comput. Phys., 257 (2014), 1-18.

[8] R.V. Craster, O.K. Matar, Dynamics and stability of thin liquid films, Rev. Mod. Phys., 81 (2009), 1131-1198.
[9] W.C. de Jesus, A.M. Roma, M.R. Pivello, M.M. Villar, A. da Silveira-Netob, A 3D front-tracking approach for simulation of a two-phase fluid with insoluble surfactant, J. Comput. Phys., 281 (2015), 403-420.
[10] M.P. do Carmo, Differential Geometry of Curves and Surfaces, Pearson, 2009.
[11] M.A. Drumright-Clarke, Y. Renardy, The effect of insoluble surfactant at dilute concentration on drop breakup under shear with inertia, Phys. Fluids, 16 (2004), 14-21.
[12] C.D. Eggleton, T.-M. Tsai, K.J. Stebe, Tip streaming from a drop in the presence of surfactants, Phys. Rev. Lett., 87 (2001), 048302.
[13] S. Frijters, F. Günther, J. Harting, Effects of nanoparticles and surfactant on droplets in shear flow, Soft Matter, 8 (2012), 6542-6556.
[14] H. Fujioka, A continuum model of interfacial surfactant transport for particle methods, J. Comput. Phys., 234 (2013), 280-294.
[15] S. Ganesan, L. Tobiska, A coupled arbitrary Lagrangian-Eulerian and Lagrangian method for computation of free surface flows with insoluble surfactants, J. Comput. Phys., 208 (2009), 2859-2873.
[16] S. Ganesan, L. Tobiska, Arbitrary Lagrangian-Eulerian finite-element method for computation of two-phase flows with soluble surfactant, J. Comput. Phys., 231 (2012), 3685-3702.
[17] S. Ganesan, Simulations of impinging droplets with surfactant-dependent dynamic contact angle, J. Comput. Phys., 301 (2015), 178-200.
[18] J.L. Guermond, P. Minev, J. Shen, An overview of projection methods for incompressible flows, Comput. Methods Appl. Mech. Engrg., 195 (2006), 6011-6045.
[19] M. Hameed, M. Siegel, Y.-N. Young, J. Li, M.R. Booty, D.T. Papageorgiou, Influence of insoluble surfactant on the deformation and breakup of a bubble or thread in a viscous fluid, J. Fluid Mech., 594 (2008), 307340.
[20] F.H. Harlow, J.E. Welsh, Numerical calculation of time-dependent viscous incompressible flow of fluid with a free surface, Phys. Fluids., 8 (1965), 2181-2189.
[21] A.J. James, J. Lowengrub, A surfactant-conserving volume-of-fluid method for interfacial flows with insoluble surfactants, J. Comput. Phys., 201 (2004), 685-722.
[22] S. Khatri, A.-K. Tornberg, A numerical method for two phase flows with insoluble surfactants, Comput. Fluids, 49 (2011), 150-165.
[23] S. Khatri, A.-K. Tornberg, An embedded boundary method for soluble surfactants with interface tracking for two-phase flows, J. Comput. Phys., 256 (2014), 768-790.
[24] I. Kralova, J. Sjöblom, Surfactants used in food industry: a review, J. Dispers. Sci. Technol., 30 (2009), 1363-1383.
[25] M.-C. Lai, Y.-H. Tseng, H. Huang, An immersed boundary method for interfacial flows with insoluble surfactant, J. Comput. Phys., 227 (2008), 7279-7293.
[26] M.-C. Lai, Y.-H. Tseng, H. Huang, Numerical simulation of moving contact lines with surfactant by immersed boundary method, Commun. Comput. Phys., 8 (2010), 735-757.
[27] M.-C. Lai, C.-Y. Huang, Y.-M. Huang, Simulating the axisymmetric interfacial flows with insoluble surfactant by immersed boundary method, Int. J. Numer. Anal. Model., 8 (2011) 105117.
[28] X. Li, C. Pozrikidis, The effect of surfactants on drop deformation and on the rheology of dilute emulsions in Stokes flow, J. Fluid Mech., 341 (1997), 165-194.
[29] H. Liu, Y. Zhang, Phase-field modeling droplet dynamics with soluble surfactants, J. Comput. Phys., 229 (2010), 9166-9187.

[30] W.J. Milliken, H.A. Stone, L.G. Leal, The effect of surfactant on transient motion of Newtonian drops, Phys. Fluids A, 5 (1993), 69-79.
[31] W.J. Milliken, L.G. Leal, The influence of surfactant on the deformation and breakup of a viscous drop: the effect of surfactant solubility, J. Colloid Interface Sci., 166 (1994), 275-285.
[32] M. Muradoglu, G. Tryggvason, A front-tracking method for computation of interfacial flows with soluble surfactants, J. Comput. Phys., 227 (2008), 2238-2262.
[33] M. Muradoglu, G. Tryggvason, Simulations of soluble surfactants in 3D multiphase flow, J. Comput. Phys., 274 (2014), 737-757.
[34] Y. Pawar, K.J. Stebe, Marangoni effects on drop deformation in an extensional flow: The role of surfactant physical chemistry. I. Insoluble surfactants, Phys. Fluids., 8 (1996), 1738-1751.
[35] C. Pozrikidis, Interfacial dynamics for Stokes flow, J. Comput. Phys., 169 (2001), 250-301.
[36] C. Pozrikidis, A finite-element method for interfacial surfactant transport, with application to the flow-induced deformation of a viscous drop, J. Eng. Math., 49 (2004), 163-180.
[37] K.-L. Pan, Y.-H. Tseng, J.-C. Chen, K.-L. Huang, C.-H. Wang, and M.-C. Lai Controlling droplet bouncing and coalescence with surfactant, J. Fluid Mech., 799, (2016), 603-636.
[38] Y. Seol, W.-F. Hu, Y. Kim, M.-C. Lai, An immersed boundary method for simulating vesicle dynamics in three dimensions, J. Comput. Phys., 322 (2016), 125-141.
[39] D. Sinclair, R. Levy, K.E. Daniels, Simulating surfactant spreading: Impact of a physically motivated equation of state, Preprint.
[40] H.A. Stone, L.G. Leal, The effects of surfactants on drop deformation and breakup, J. Fluid Mech., 220 (1990), 161-186.
[41] H.A. Stone, A simple derivation of the time-dependent convective-diffusion equation for surfactant transport along a deforming interface, Phys. Fluids A., 2 (1) (1990), 111-112.
[42] S.L. Strickland, M. Hin, M.R. Sayanagi, C. Gaebler, K.E. Daniels, R. Levy, Self-healing dynamics of surfactant coatings on thin viscous films, Phys. Fluids., 26 (2014), 042109.
[43] K.E. Teigen, P. Song, J. Lowengrub, A. Voigt, A diffuse-interface method for two-phase flows with soluble surfactants, J. Comput. Phys., 203 (2011), 375-393.
[44] L.N. Trefethen, Spectral Methods in MATLAB, SIAM, Philadelphia, 2000.
[45] G. Tryggvason, R. Scardovelli, S. Zaleski, Direct numerical simulations of gas-liquid multiphase flows, Cambridge University Press, 2011.
[46] T.M. Tsai, M.J. Miksis, The effects of surfactant on the dynamics of bubble snap-off, J. Fluid Mech., 337 (1997), 381-410.
[47] J.-J. Xu, Z. Li, J. Lowengrub, H. Zhao, A level-set method for interfacial flows with surfactant, J. Comput. Phys., 212 (2006), 590-616.
[48] J.-J. Xu, Y. Yang, J. Lowengrub, A level-set continuum method for two-phase flows with insoluble surfactant, J. Comput. Phys., 231 (2012), 5897-5909.
[49] J.-J. Xu, Y. Huang, M.-C. Lai, Z. Li, A coupled immersed interface and level set method for three-dimensional interfacial flows with insoluble surfactant, Commun. Comput. Phys., 15 (2014), 451-469.
[50] X. Yang, X. Zhang, Z. Li, G.-W. He, A smoothing technique for discrete delta functions with application to immersed boundary method in moving boundary simulations, J. Comput. Phys., 228 (2009), 7821-7836.
[51] S. Yon, C. Pozrikidis, A Finite-volume/Boundary-element Method for Flow Past Interfaces in the Presence of Surfactants, with Application to Shear Flow Past a Viscous Drop, Comput. Fluids, 27 (1998), 879-902.